Proceedings of the 2006 IEEE International Conference on Robotics and Automation
Orlando, Florida - May 2006

Analysis of Two 3-DOF Parallel Mechanisms with Constrained Stewart Platform Structure

Seok-Hee Lee and Whee-Kuk Kim

Department of Control and Instrumentation Engineering

Korea University
South Korea

{idwestkey, wheekuk}@korea.ac.kr

Byung-Ju Yi and Il-Hong Suh[1]

School of Electrical Engineering and Computer Science
Department of Information and Communication[1]
Hanyang University
South Korea

{bj,ihsuh}@hanyang.ac.kr

***Abstract* - Two 3-DOF parallel mechanisms, a translational mechanism and a spherical mechanism, are analyzed. Each of two mechanisms commonly possesses three UPS serial sub-chains, and an additional passive 3-DOF PPP-type serial sub-chain and a passive 3-DOF RRR-type serial sub-chain are incorporated for the translational device and the rotational device, respectively. Such additional passive serial sub-chains act as constraints to restrict the output motion of the mechanism either in a 3-DOF translational space or in a 3-DOF spherical space. The position solutions of the proposed mechanisms and their first-order kinematic models are derived. Then their workspaces and kinematic characteristics are examined via the kinematic isotropic index.**

Index Terms* - *Stewart Platform, Parallel Mechanism, Position Analysis, Kinematic Analysis, Kinematic Isotropic Index

I. Introduction

It is known that parallel mechanisms bear higher stiffness characteristics and better accuracy compared to the serial mechanism. Also, actuator locations in the mechanism could be placed toward the ground, and thus this reduces the dynamic effect due to floating actuators significantly. However, due to its intrinsically constrained links in its structure much more complicated analyses are involved in its kinematic and dynamic analysis. Nonetheless, parallel mechanism, typically such as a Stewart Platform structure, has been recognized as excellent candidates for applications such as a flight simulator and has been employed in other applications requiring higher load and higher accuracy.[1-3]

Recent research works also involve design and analysis for less degree-of-freedom devices having 3, 4, and 5 DOF[4-9]. One early example is a novel translational 3-DOF parallel mechanism employing UPU chain structure [4,5]. Tsai, et al.[6] proposed a 3 DOF translational device which has local four-bar loops. Joshi and Tsai [7] proposed another 3 DOF parallel mechanism having three sub chains and one supporting leg. Tsai, et al [8] also proposed 4- and 5-DOF parallel mechanism using supporting leg at the center of mechanisms. Kim, et al [10] proposed a 3 DOF device which has unique forward solution but multiple reverse solutions. It is noted, however, that previous 3 DOF parallel devices have neither closed form forward solution nor inverse solution. Therefore, in this paper, we investigated two different mechanism nodules, one of which is a translational 3 DOF mechanisms having a closed-form solution in the forward and reverse position analysis. Their basic structures are similar to the Stewart Platform structure but have an additional supporting leg at the center of the mechanism, which constrains the output motion space of the Stewart Platform mechanism as desired. After their structures being described, the forward and reverse position solutions of the two proposed mechanisms are discussed in detail. Then their workspaces and their kinematic characteristics are examined via kinematic isotropic index.

II. Position Analyses

A. Description of mechanisms

As shown in Fig. 1, the mechanism is formed with three identical UPS sub chains and an additional *PPP* sub chain at the center of the mechanism. Denote the base coordinates located at the center of the lower plate and the output coordinate located at the center of the upper plate as $(x_b \quad y_b \quad z_b)$ and $(x_t \quad y_t \quad z_t)$, respectively.

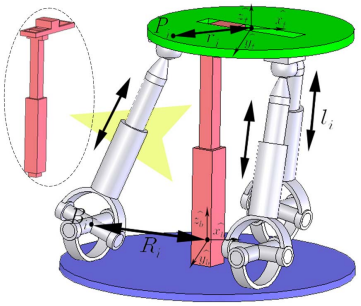

Fig. 1 A 3 DOF translational mechanism

Three universal joints are placed on the circle of radius R on the base plate with an interval of $120°$. And one end of each of prismatic joints is connected to the corresponding universal joint and the other end to the spherical joint fixed on the upper plate as shown in Fig. 1. The mobility of the mechanism could be confirmed from well-known Grubler's mobility formula as below :

$$\begin{aligned} M &= d(l-1) - \sum_i c_i \\ &= 6(10-1) - (3\times 3 + 4\times 3 + 6\times 5) \\ &= 3 \end{aligned} \tag{1}$$

where d represents the admissible motion space of all joints which is counted as 6 in this example, and l and c_i represents the number of links including the ground and the number of constraints imposed to the joint i, respectively. Table 1 shows the D-H(Denavit Hartenberg) link parameters for one *RRPS* sub-chain of the mechanism. The other sub-chains could be easily found similarly and omitted for simplicity.

TABLE I
DENAVIT HARTENBERG LINK PARAMETERS OF A SERIAL SUB-CHAIN

Link	${}_i\alpha_{jk}$	α_{jk}	${}_i s_{jj}\,({}_i l_j)$	${}_i\phi_j$
Base Plate	0°	R	0	γ_{bi}
Link # 1	–90°	0°	0	${}_i\phi_1$
Link # 2	90°	0°	0	${}_i\phi_2$
Link # 3	–90°	0°	l_i	${}_i\phi_3$
Link # 4	90°	0°	0	${}_i\phi_4$
Link # 5	90°	0°	0	${}_i\phi_5$
Link # 6	90°	0°	0	${}_i\phi_6$
Top Plate	0°	$-r$	0	γ_{ti}

Now, denote the absolute position vector from the origin of the base coordinate frame to the universal joint of the i^{th} serial sub-chain as $\mathbf{R_i}$ ($i = 1, 2, 3$). More specifically, the position vector $\mathbf{R_i}$ can be expressed explicitly as below, based on the definition in Table 1:

$$\mathbf{R_i} = [R\cos(\gamma_{bi}^b) \quad R\sin(\gamma_{bi}^b) \quad 0]^T, \tag{2}$$

where γ_{bi}^b represents the offset angle between $\mathbf{x_b}$ and $\mathbf{R_i}$ about the $\mathbf{z_b}$ axis. Similarly, let $\mathbf{P_i}$ ($i = 1, 2, 3$) denote the absolute position vector from the origin of the base frame to the spherical joint of the i^{th} sub-chain. Assume that the spherical joints are placed on the circle of radius of r on the upper plate with an uniform interval of 120° among them. Then the local position vector from the origin of the output frame to the point P_i, $\mathbf{r_i^{(t)}}$ for $i = 1, 2, 3$, can be expressed as

$$\begin{aligned}\mathbf{r_i^{(t)}} &= (r_{ix}^{(t)}, \quad r_{iy}^{(t)}, \quad r_{iz}^{(t)})^T \\ &= (r\cos(\gamma_{ti}^t), \quad r\sin(\gamma_{ti}^t), \quad 0)^T\end{aligned} \tag{3}$$

where γ_{ti}^t represents the offset angle between $\mathbf{x_t}$ and $\mathbf{r_i}$ about $\mathbf{z_t}$ axis, respectively. As in Fig. 2, denote the position vector from the point B_i to the point P_i as $\mathbf{l_i}$. l_i, a variable of the prismatic joint of the i^{th} sub-chain, represents the distance from the point B_i to the point P_i.

The structure of the spherical mechanism is similar to that of the translational mechanism mentioned above. Only difference is that the spherical mechanism has an *RRR*-type additional sub-chain instead of an *PPP*-type sub-chain of the translational mechanism. Thus, the above description and mobility analysis for the translational mechanism can be applied identically to the spherical mechanism.

The output position of the translational mechanism (the origin of the output frame) is denoted as $\mathbf{R_t} = [x_t \quad y_t \quad z_t]^T$. However, the output orientation of the translational mechanism is fixed due to the additional *PPP* sub-chain and will be assumed to be $[I]_{3\times3}$ for convenience. On the other hand, the spherical mechanism has a fixed output position denoted as $\mathbf{R_t} = [x_t \quad y_t \quad z_t]^T = [0 \quad 0 \quad z_t]^T$, which becomes a hinge point for the rotational motion. The output orientation of the spherical mechanism is defined using three Euler angles and its rotational output matrix with respect to the base frame, $[R_b^t]$, can be expressed as below :

$$\begin{aligned}[R_b^t] &= [Rot(\mathbf{x}, \alpha)][Rot(\mathbf{y}, \beta)][Rot(\mathbf{z}, \gamma)] \\ &= \begin{bmatrix} c_\beta c_\gamma & -c_\beta s_\gamma & s_\beta \\ s_\alpha s_\beta c_\gamma + c_\alpha s_\gamma & -s_\alpha s_\beta s_\gamma + c_\alpha c_\gamma & -s_\alpha c_\beta \\ -c_\alpha s_\beta c_\gamma + s_\alpha s_\gamma & c_\alpha s_\beta s_\gamma + s_\alpha c_\gamma & c_\alpha c_\beta \end{bmatrix}\end{aligned} \tag{4}$$

B. Position Analyses of the translational mechanism

1. Reverse Position Analysis

The absolute position from the origin of the base frame to the origin of the output frame can be expressed as

$$\mathbf{P} = \mathbf{R_i} + l_i\hat{\mathbf{l}}_\mathbf{i} - \mathbf{r_i} \tag{5}$$

where

$$\begin{aligned}&\mathbf{r_i} = [R_b^t]\mathbf{r_i^{(t)}}, \\ &\mathbf{P} = (x, \ y, \ z)^T, \\ &\mathbf{R_i} = (R_{ix}, \ R_{iy}, \ R_{iz})^T, \\ &\mathbf{r_i^{(t)}} = (r_{ix}^{(t)}, \ r_{iy}^{(t)}, \ r_{iz}^{(t)})^T.\end{aligned} \tag{6}$$

Note particularly that as discussed previously, the output orientation of the upper plate is assumed to be a unit matrix in the translational device,

$$[R_b^t] = [I_{3\times3}]. \tag{7}$$

Using these assumptions, (5) can be rewritten as

$$\mathbf{P} = \mathbf{R_i} + l_i\hat{\mathbf{l}}_\mathbf{i} - \mathbf{r_i^{(t)}}. \tag{8}$$

After rearranging (8), we have

$$l_i\hat{\mathbf{l}}_\mathbf{i} = \mathbf{P} - \mathbf{R_i} + \mathbf{r_i^{(t)}}, \tag{9}$$

Now, taking inner product to the both sides of (9) gives

$$\begin{aligned}l_i\hat{\mathbf{l}}_\mathbf{i} \cdot l_i\hat{\mathbf{l}}_\mathbf{i} &= l_i^2 = (\mathbf{P} - \mathbf{R_i} + \mathbf{r_i^{(t)}})^T(\mathbf{P} - \mathbf{R_i} + \mathbf{r_i^{(t)}}) \\ &= \mathbf{P}^T\mathbf{P} + \mathbf{R_i}^T\mathbf{R_i} + \mathbf{r_i^{(t)T}}\mathbf{r_i^{(t)}} - 2\mathbf{R_i}^T\mathbf{P} - 2\mathbf{R_i}^T\mathbf{r_i^{(t)}} + 2\mathbf{P}^T\mathbf{r_i^{(t)}}\end{aligned} \tag{10}$$

where

$$\mathbf{R_i}^T\mathbf{R_i} = R_i^2,$$

$$\mathbf{P}^T\mathbf{P} = x^2 + y^2 + z^2,$$
$$\mathbf{r_i^{(t)T}}\mathbf{r_i^{(t)}} = r_i^2,$$
$$\mathbf{R_i}^T\mathbf{P} = R_{ix}x + R_{iy}y + R_{iz}z, \tag{11}$$
$$\mathbf{R_i}^T\mathbf{r_i^{(t)}} = R_{ix}r_{ix}^{(t)} + R_{iy}r_{iy}^{(t)} + R_{iz}r_{iz}^{(t)},$$
$$\mathbf{P}^T\mathbf{r_i^{(t)}} = xr_{ix}^{(t)} + yr_{iy}^{(t)} + zr_{iz}^{(t)}.$$

Again, further simplifying (10) yields the final form for the reverse solution as below :

$$l_i^2 = x^2 + y^2 + z^2 + R_i^2 + r_i^2 - 2(R_{ix} - r_{ix})x - 2(R_{iy} - r_{iy})y - 2(R_{iz} - r_{iz})z - 2(R_{ix}r_{ix}^{(t)} + R_{iy}r_{iy}^{(t)} + R_{iz}r_{iz}^{(t)}) \tag{12}$$

Once the desired output position vector $P = (x \quad y \quad z)^T$ is given, the required input (that is, the prismatic joint variables) can directly be calculated from (12).

2. Forward Position Analysis

Given the displacement information for the three linear joints, the position of the platform will be estimated.

(12) can be rearranged as follows :

$$x^2 + y^2 + z^2 + R_i^2 + r_i^2 - l_i^2 - 2(R_{ix} - r_{ix})x - 2(R_{iy} - r_{iy})y - 2(R_{iz} - r_{iz})z - 2(R_{ix}r_{ix}^{(t)} + R_{iy}r_{iy}^{(t)} + R_{iz}r_{iz}^{(t)}) = 0, \quad for\ i = 1, 2, 3. \tag{13}$$

Subtracting the second and third equation, respectively, from the first equation in (13) and noting that $\mathbf{R_1}^T\mathbf{r_1^{(t)}} = \mathbf{R_2}^T\mathbf{r_2^{(t)}} = \mathbf{R_3}^T\mathbf{r_3^{(t)}}$, the results can be written as follows:

$$2[(R_{1x} - r_{1x}) - (R_{2x} - r_{2x})]x + 2[(R_{1y} - r_{iy}) - (R_{2y} - r_{2y})]y = l_2^2 - l_1^2 \tag{14}$$

$$2[(R_{1x} - r_{1x}) - (R_{3x} - r_{3x})]x + 2[(R_{1y} - r_{iy}) - (R_{3y} - r_{3y})]y = l_3^2 - l_1^2 \tag{15}$$

Particularly, note that since $\mathbf{R_i}$ and $\mathbf{r_i^{(t)}}$ are known, the displacements of all three prismatic joints in Eqs. (14) and (15) are also known values.

Now, (14) and (15) can be written in a matrix form as below :

$$[A]\begin{bmatrix} x \\ y \end{bmatrix} = \begin{bmatrix} l_2^2 - l_1^2 \\ l_3^2 - l_1^2 \end{bmatrix} \tag{16}$$

where

$$[A] = \begin{bmatrix} A_{11} & A_{12} \\ A_{21} & A_{22} \end{bmatrix}$$
$$A_{11} = 2[(R_{1x} - r_{1x}) - (R_{2x} - r_{2x})] \tag{17}$$
$$A_{12} = 2[(R_{1y} - r_{1y}) - (R_{2y} - r_{2y})]$$
$$A_{21} = 2[(R_{1x} - r_{1x}) - (R_{3x} - r_{3x})]$$
$$A_{22} = 2[(R_{1y} - r_{1y}) - (R_{3y} - r_{3y})]$$

When the matrix $[A]$ is not singular, the output variables, x and y, can be computed by taking the inverse of (16) as follows :

$$\begin{bmatrix} x \\ y \end{bmatrix} = [A]^{-1}\begin{bmatrix} l_2^2 - l_1^2 \\ l_3^2 - l_1^2 \end{bmatrix} \tag{18}$$

The remaining output variable z can also be found by inserting the values of x and y into any equation of (13) :

$$z^2 + az + b = 0$$

where

$$a = -2(R_{iz} - r_{iz}), \tag{19}$$
$$b = x^2 + y^2 + R_i^2 + r_i^2 - l_i^2 - 2(R_{ix} - r_{ix})x - 2(R_{iy} - r_{iy})y - 2(R_{ix}r_{ix}^{(t)} + R_{iy}r_{iy}^{(t)} + R_{iz}r_{iz}^{(t)}).$$

It can be seen from (19) that there are two solutions for z. However, it is easily noticeable that these solutions represent the mirror images with respect to the x - y plane. Thus, a unique forward solution can be obtained.

C. Position Analyses of the spherical mechanism

1. Reverse Position Analysis

For the 3 DOF rotational device in Fig 2, the position vector from the origin of the base frame to the origin of the output frame can be expressed as

$$\mathbf{P} = \mathbf{R_i} + l_i\hat{\mathbf{l}}_\mathbf{i} - \mathbf{r_i} \tag{20}$$

where

$$\mathbf{P} = (x,\ y,\ z)^T,$$
$$\mathbf{R_i} = (R_{ix},\ R_{iy},\ R_{iz})^T, \tag{21}$$
$$\mathbf{r_i^{(t)}} = (r_{ix}^{(t)},\ r_{iy}^{(t)},\ r_{iz}^{(t)})^T.$$

After rearranging (20) with respect to $l_i\hat{\mathbf{l}}_\mathbf{i}$, we have

$$l_i\hat{\mathbf{l}}_\mathbf{i} = \mathbf{P} - \mathbf{R_i} + \mathbf{r_i}, \tag{22}$$

Taking the inner product to the both side of (22) yields

$$l_i^2 = l_i\hat{\mathbf{l}}_\mathbf{i} \cdot l_i\hat{\mathbf{l}}_\mathbf{i} = (\mathbf{P} - \mathbf{R_i} + \mathbf{r_i})^T(\mathbf{P} - \mathbf{R_i} + \mathbf{r_i}) \tag{23}$$
$$= \mathbf{P}^T\mathbf{P} + \mathbf{R_i}^T\mathbf{R_i} + \mathbf{r_i}^T\mathbf{r_i} - 2\mathbf{R_i}^T\mathbf{P} - 2\mathbf{R_i}^T\mathbf{r_i} + 2\mathbf{P}^T\mathbf{r_i}$$

Inserting the following definitions into (23)

$$\mathbf{R_i}^T\mathbf{R_i} = R_i^2,$$
$$\mathbf{P}^T\mathbf{P} = x^2 + y^2 + z^2,$$
$$\mathbf{r_i}^T\mathbf{r_i} = r_i^2,$$
$$\mathbf{R_i}^T\mathbf{P} = R_{ix}x + R_{iy}y + R_{iz}z, \tag{24}$$
$$\mathbf{R_i}^T\mathbf{r_i} = R_{ix}r_{ix} + R_{iy}r_{iy} + R_{iz}r_{iz},$$

$$\mathbf{P}^T\mathbf{r_i} = xr_{ix} + yr_{iy} + zr_{iz},$$

$$\mathbf{r_i} = [R_b^t]\mathbf{r_i^{(t)}}.$$

rearranging the results yields

$$\begin{aligned} l_i^2 &= x^2 + y^2 + z^2 + R_i^2 + r_i^2 \\ &\quad - 2R_{ix}x - 2R_{iy}y - 2R_{iz}z \\ &\quad + 2[(x - R_{ix}), (y - R_{iy}), (z - R_{iz})]([R_b^t]\mathbf{r_i^{(t)}}) \end{aligned} \tag{25}$$

Note that R_{ix}, r_i, x, y, z in (25) are fixed design parameters. Thus, when the output vector represented by Euler angle as in (4), $\mu = (\alpha \quad \beta \quad \gamma)^T$, is given, the corresponding input vector of prismatic joint displacements can directly be calculated from (25)

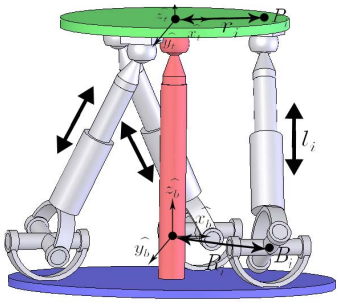

Fig. 2 A 3 DOF spherical mechanism

2. Forward Position Analysis

Given the displacement information for the three linear joints, the orientation of the platform will be estimated. This problem for this type of mechanisms is well discussed in [8] and will not addressed here.

III. Kinematic Analyses

A. The Translation 3-DOF Mechanism

1. First-order Kinematic Analysis

Directly differentiating (12) with respect to time and rearranging the results yields the following reverse input-output velocity relationship

$$\dot{\mathbf{l}} = [G_u^l]\dot{\mathbf{u}}, \tag{26}$$

where

$$[G_u^l] = \begin{bmatrix} g_{11} & g_{12} & g_{13} \\ g_{21} & g_{22} & g_{23} \\ g_{31} & g_{32} & g_{33} \end{bmatrix} \tag{27}$$

and for $i = 1, 2, 3$,

$$g_{i1} = \frac{2x - 2(R_{ix} - r_{ix})}{2l_i}$$

$$g_{i2} = \frac{2y - 2(R_{iy} - r_{iy})}{2l_i} \tag{28}$$

$$g_{i3} = \frac{2z - 2(R_{iz} - r_{iz})}{2l_i}.$$

Assuming that the matrix $[G_u^l]$ is nonsingular, the forward velocity relationship between the input and the output can be represented as

$$\dot{\mathbf{u}} = [G_l^u]\dot{\mathbf{l}}, \tag{29}$$

where

$$[G_l^u] = [G_u^l]^{-1}. \tag{30}$$

It can be seen from (27) that when $R_i = r_i$ for all $i = 1, 2, 3$ the matrix $[G_u^l]$ becomes a null matrix, implying singular configuration.

2. First-order Kinematic Characteristics

In this section, the workspace size and the first order kinematic characteristics of the mechanism will be investigated. To examine the kinematic characteristics, the kinematic isotropic index defined as below will be employed :

$$\sigma_{KI} = \frac{\sigma_{\min}([G_l^u])}{\sigma_{\max}([G_l^u])}, \tag{31}$$

where $\sigma_{\min}([G_l^u])$ and $\sigma_{\max}([G_l^u])$ denote the minimum and minimum singular value of $[G_l^u]$, respectively. The index represents the level of the uniformity of the input-output velocity transmission ratio of the mechanism at that configuration. Particularly, when index goes to unit value, it represents perfect isotropic configuration of the mechanism.

Without the loss of generality, in the following simulation it is assumed that the radius of the base plate R has a unit magnitude and the strokes of the prismatic joints l_i are limited within the range of $0.5 \le l_i \le 2$. And to take advantage of the geometric symmetry of the mechanism the offset angles are selected as follows :

$$\gamma_{bi}^b = (i-1)\times 120°, \quad for \quad i = 1, 2, 3 \tag{32}$$

$$\gamma_{ti}^b = (i-1)\times 120°, \quad for \quad i = 1, 2, 3. \tag{33}$$

The effects of one design parameter r and output variables on the kinematic characteristics throughout its workspace are examined. Particularly, since the contour plot can provide visual image on the plane of only two output variables, various contour plots for step-wise values of the other remaining output variable, namely z_t, are obtained in the following simulations.

Fig. 3 shows the 3-D plot and the contour plot of the maximum and minimum values for two output variables, z_t (that is, $z_{t\max}$ and $z_{t\min}$) on the $x-y$ plane when the radius

of the upper plate is set to be $r = 0.75$. For brevity, the rough boundary of the workspace in the figure is shown as the contour line of kinematic isotropic index σ_{KI} equal to or above 0.01. The rough size of the workspace can also be estimated in the figure. From this figure, it can be confirmed that the workspace of the proposed mechanism is fairly large. Fig. 4 shows the contour plot the kinematic isotropic index on the $x-y$ plane when $r = 0.25$ and $z_t = 0.5, 1.0, 1.5$, respectively. Similarly, Fig. 5 shows the contour plot of the kinematic isotropic index on the $x-y$ plane when $r = 0.5$ and $z_t = 0.5, 1.0, 1.5$, respectively. And Fig. 6 shows the contour plots the kinematic isotropic index on the $x-y$ plane when $r = 0.75$ and $z_t = 0.5, 1.0, 1.5$, respectively. From these plots the approximate 3-shape and size of the workspace of the mechanism for those specified design parameters can be inferred in addition to its kinematic isotropic properties. Also, it can be observed from these results that the size of the workspace is related to the ratio of the radii of the upper plate and the lower plate. Particularly, note that it can be inferred that when $[R_b^t] = [I]$, the kinematic isotropic index has its maximum at the center area of the plots.

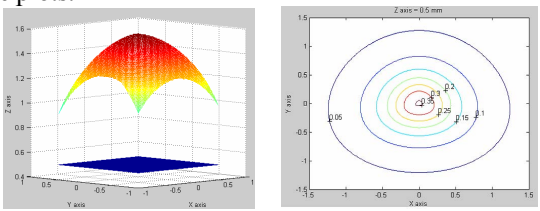

(a) Boundary of 3-D workspace for z-max(red) and z-min(blue).
(b) Contour plot for z-max

Fig. 3. Workspace analysis

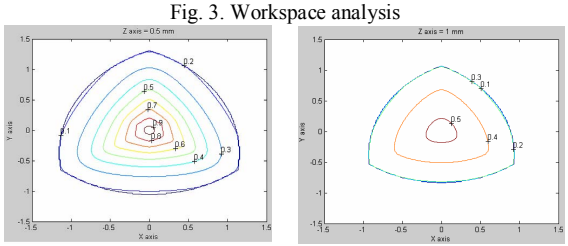

(a) $z_t = 0.5$ (b) $z_t = 1.0$

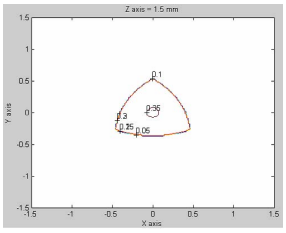

(c) $z_t = 1.5$

Fig. 4. Contour plots when $r = 0.25$

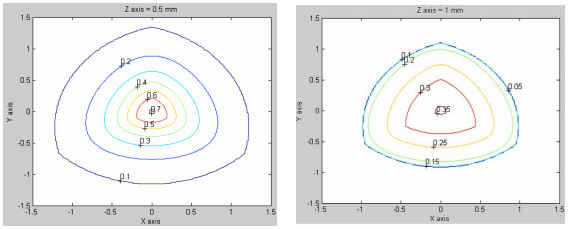

(a) $z_t = 0.5$ (b) $z_t = 1.0$

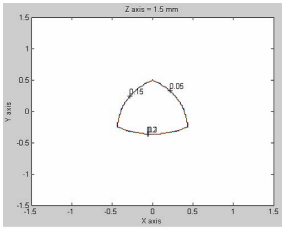

(c) $z_t = 1.5$

Fig. 5. Contour plots when $r = 0.5$

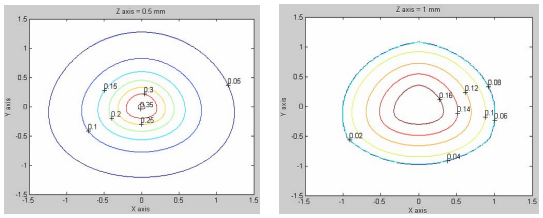

(a) $z_t = 0.5$ (b) $z_t = 1.0$

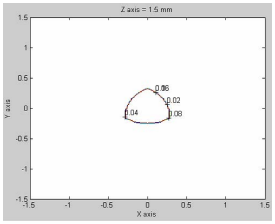

(c) $z_t = 1.5$

Fig. 6. Contour plots when $r = 1.5$

B. The Spherical 3-DOF Mechanism

1. First-order Kinematic Analysis

By following the same procedure as the section III-A, the forward and reverse velocity relationship for the spherical mechanism can be found.

2. First-order Kinematic Characteristics

The parameters used in this simulation are exactly the same as discussed in section III-A-2. Effects of one design parameter γ and output variables on the kinematic characteristics throughout its workspace are examined. Again, since the contour plot can provide visual image on the plane of only two output variables, various contour plots for step-wise values of the other remaining output variable, namely γ, are obtained in the following simulations. Also, for simplicity, it is assumed that the hinge point for the rotational motion is fixed at $(x_t, y_t, z_t) = (0, 0, 1)$ in the following simulations.

Fig. 7 shows the 3-D plot and contour plot of the maximum and the minimum values for the output variables, γ (that is, $\gamma_{\max}$ and $\gamma_{\min}$) on the $\alpha-\beta$ plane when the radius of the upper plate is set to be $r=0.75$. For brevity, the rough boundary of the workspace in the figure is identified as the contour line of the kinematic isotropic index σ_{KI} equal to or above 0.01. The approximate size and shape of the workspace can be seen through these figures and it can also be confirmed that the workspace of the proposed mechanism is fairly large.

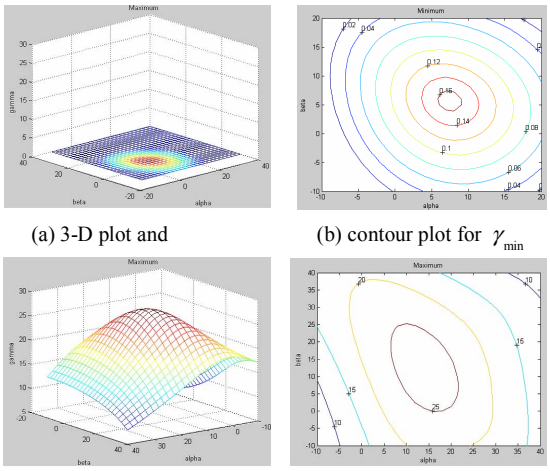

(a) 3-D plot and (b) contour plot for $\gamma_{\min}$

(c) 3-D plot (d) contour plot for $\gamma_{\max}$

Fig. 7. Workspace of the rotational mechanism when $r=0.75$

Fig. 8 shows the contour plot for the kinematic isotropic index on the $\alpha-\beta$ plane when $r=0.25$ and $\gamma=20°,\ 40°,\ 60°$, respectively. Similarly, Fig. 9 shows the contour plot for the kinematic isotropic index on the $\alpha-\beta$ plane when $r=0.5$ and $\gamma=20°,\ 40°,\ 60°$, respectively. And Fig. 10 shows the contour plot for the kinematic isotropic index on the $\alpha-\beta$ plane when $r=0.75$ and $\gamma=20°,\ 40°,\ 60°$, respectively. From these plots, it can be observed that the size of the workspace is also related to the ratio of the radii of the upper plate and the lower plate.

The result of the above kinematic analysis for both mechanisms will be useful, preliminary data for optimal design of these mechanisms.

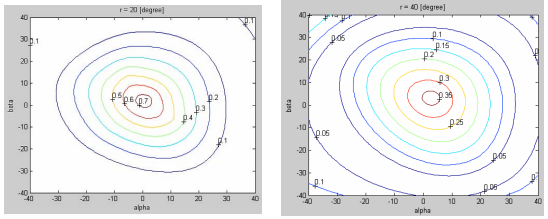

(a) $\gamma=20°$ (b) $\gamma=40°$

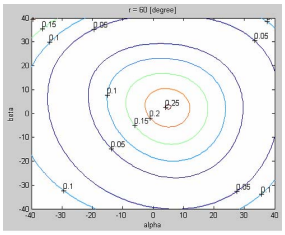

(c) $\gamma=60°$

Fig. 8. Contour plots when $r=0.25$

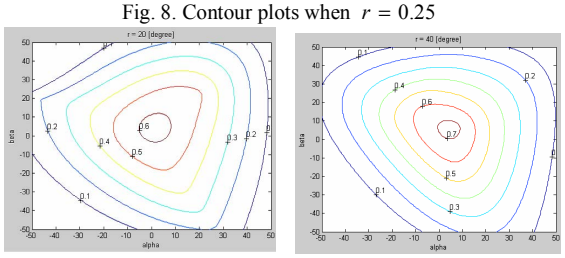

(a) $\gamma=20°$ (b) $\gamma=40°$

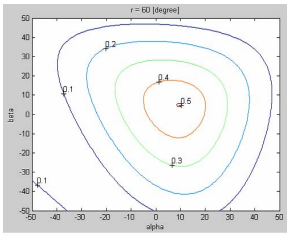

(c) $\gamma=60°$

Fig. 9. Contour plots when $r=0.5$

VI. Conclusions

The position solutions and the first-order kinematic models of two different 3-DOF parallel mechanisms, a translational and a spherical, are discussed. And using kinematic isotropic index their kinematic characteristics are examined. Through simulations, it is confirmed that both proposed mechanisms have fairly large workspace and good kinematic properties. Noting that both mechanisms have very good kinematic characteristics despite of its parallel structure along with their decoupled 3-dof output characteristics(i.e., pure spherical and translational, respectively), it can be contended that both mechanisms have high potential of wide applications requiring high payload and high precision not only as a single manipulator but also as modules in constructing more complex hybrid manipulators[11-12].

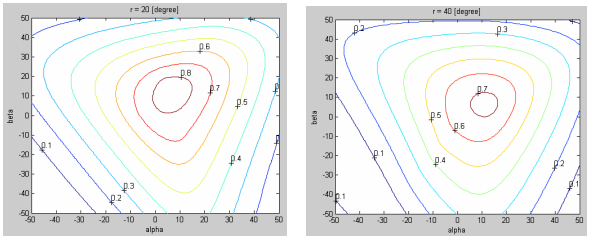

(a) $\gamma=20°$ (b) $\gamma=40°$

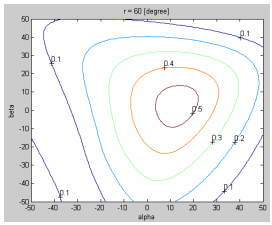

(c) $\gamma = 60°$

Fig. 10. Contour plots when $r = 0.75$

REFERENCES

[1] D. Stewart, "A Platform with Six Degree of Freedom," Proceedings of the Institute of Mechanical Engineering, Vol. 180, Part 1, no. 15, pp. 371-386, 1965.

[2] W.K. Kim, K.K.Huh, B.-J. Yi, "Kinemaitc/Dynamic Optimal Design of A Stewart Platform Mechanism," Journal of Control, Automation and Systems Engineering, Vol. 2, No. 1, pp. 45-52, March, 1996.

[3] W.K. Kim, Y.K. Byun, H.S. Cho, "Closed-Form Solution of Forward Position Analysis for a 6-DoF 3-PPSP Parallel Mechanism and Its Implementation", International Journal of Robotics Research, vol. 20, no. 1, pp. 85-99, Jan. 2001.

[4] K.M. Lee and D.K. Shah, "Kinematic Analysis of a Three Degrees of Freedom In-Parallel Actuated Manipulator, Proceedings of IEEE Int'l conf. of Robotics and Automation, pp. 345-350, 1987.

[5] K.M. Lee and D.K. Shah, "Dynamic Analysis of a Three-Degrees-of-Freedom In-Parallel Actuated Manipulator," IEEE Trans. on Journal of Robotics and Automation, Vol. 4, no. 3, pp. 361-367, June 1988.

[6] L.-W. Tsai, G.C. Walsh, and R.E. Stamper, "Kinematics of a Novel Three DOF Translational Platform," Proceedings of IEEE Int. Conf. on Robotics and Automation, pp. 3446-3451, 1996.

[7] S. Joshi and L.-W. Tsai, "A Comparison Study of Two 3-DOF Parallel Manipulators: One with Three and the Other with Four Supporting Legs," Proceedings of IEEE Int'l Conf. on Robotics and Automation, pp. 3690-3697, 2002.

[8] L.W.Tsai, "Robot Analysis : the mechanics of serial and parallel manipulators," John Wiley & Sons Inc., 1999.

[9] J.P.Merlet, "Parallel Robots," Kluwer Academic Publishers, 2000.

[10] W.K. Kim, J.Y. Lee, and B.-J. Yi, "Analysis on Kinematic Characteristics of Two Types of 3 Degree-of-Freedom Parallel Manipulators," Proceedings of Robotics. System & Automation Conf., Korea, April, 1996.

[11] D. Yi, B.-J. Yi, and W.K. Kim, "Design of a New Grasper Mechanism Having XYZ Translational Motions," Proceedings of IEEE Int. Conf. on Robotics and Automation, pp. 690-695, 2003.

[12] Z. Mingayng, et. al., "Development of A Redundant Robot Manipulator Based on Three DOF Parallel Platforms," Proceedings of IEEE Int'l Conf. on Robotics and Automation, pp. 221-226, 1995.